Available online at www.sciencedirect.com
SCIENCE DIRECT®
Journal of Solid State Chemistry 175 (2003) 59–62
JOURNAL OF SOLID STATE CHEMISTRY
http://elsevier.com/locate/jssc

Normal micelle synthesis and characterization of $MgAl_2O_4$ spinel nanoparticles

Christy R. Vestal and Z. John Zhang*

School of Chemistry and Biochemistry, Georgia Institute of Technology, Atlanta, GA 30332-0400, USA

Received 1 December 2002; received in revised form 1 March 2003; accepted 3 March 2003

Abstract

Magnesium–aluminum oxide, $MgAl_2O_4$ spinel nanoparticles have been synthesized using normal micelle microemulsion methods. A mixed magnesium–aluminum hydroxide is initially formed which after annealing at 600°C forms nanocrystalline $MgAl_2O_4$ spinel. By controlling reactant concentration in the micelle solution, the particle size has been tuned over the range 4–20 nm. The reaction pathways have been determined by using the characterization methods such as X-ray diffraction, thermogravimetric analysis and differential scanning calorimetry.

Keywords: Micelle synthesis; Spinel nanoparticles

1. Introduction

Spinel proper, $MgAl_2O_4$ is used in a wide range of applications such as catalysis and sensors [1–3]. For many of its applications, a high surface area is greatly desired. Nanometer-sized spinel particles certainly offer great advantages for the fulfillment of this requirement [4]. Nanosize spinel particles have been previously prepared by methods of sol–gel, spray-drying, complexation, co-precipitation, and decomposition of metal alkoxides as well [5–8]. Although these synthesis routes produce nanosized particles, ease of tuning particle size is hardly to be achieved. Furthermore, most of the above-described methods require employing costly equipment. The expensive and moisture-sensitive precursors in these methods also drive up the cost greatly for producing large quantities of high surface area $MgAl_2O_4$ powders.

Over the past decade, microemulsion synthesis methods utilizing normal micelles have emerged as a versatile route to form a wide range of nanoparticle materials. Metal (e.g., Cu), semiconductor (e.g., CdS), and spinel ferrite (e.g., $CoFe_2O_4$) nanoparticles with low size dispersity have been prepared using this method [9–12]. One advantage of this versatile method is that the nanoparticle size can be easily adjusted by small condition changes in the synthesis procedure. For example, chemometric modeling has shown that adjusting the metal cation concentration and the reaction temperature allow control over the size of spinel ferrite nanoparticle [13]. The feasibility of using these simple synthesis adjustments to control nanoparticle size was demonstrated for a range of spinel ferrite nanoparticles—$CoFe_2O_4$, $ZnFe_2O_4$, and $MgFe_2O_4$, which possess unique and important magnetic properties. $MgAl_2O_4$ spinel nanoparticles are non-magnetic. However, they have the same features in terms of crystallographic structures, chemical coordinations and bonding. Moreover, the topographic surface of the nanoparticles is the same. The successful synthesis of $MgAl_2O_4$ spinel nanoparticles using similar microemulsion methods will help us in understanding of magnetic properties of spinel ferrite nanoparticles at the atomic level.

We here report the use of normal micelle microemulsion methods for the synthesis of $MgAl_2O_4$ nanoparticles. This aqueous method uses readily available, inexpensive, and easily handled precursors of $Mg(NO_3)_2$ and $Al(NO_3)_3$, and eliminates the extra handling requirements that usually associate with moisture sensitive precursors. Furthermore, using the chemometric model developed in normal micelle microemulsion methods for size control synthesis of spinel ferrite MFe_2O_4 nanoparticles, the size of the $MgAl_2O_4$

*Corresponding author. Fax: +1-404-894-7452.
E-mail address: john.zhang@chemistry.gatech.edu (Z.J. Zhang).

0022-4596/03/$ - see front matter © 2003 Elsevier Science (USA). All rights reserved.
doi:10.1016/S0022-4596(03)00143-9

nanoparticles can be tuned by minor adjustments to the synthesis conditions.

2. Experimental

2.1. Nanoparticle synthesis

A normal micelle microemulsion method was used to prepare $MgAl_2O_4$ spinel nanoparticles. Aqueous solutions of $Mg(NO_3)_2$ (Fisher, 0.008 M) and $Al(NO_3)_3$ (Fisher, 0.016 M) were added to an aqueous solution sodium dodecyl sulfate (Aldrich, 0.090 M) to form the normal micelles. NH_4OH (Fisher, 30 wt%) was added dropwise until the pH reached ~10.3, and then the solution was stirred overnight. Ethanol was added to flocculate the particles and the precipitate was collected by centrifugation. The samples were dried in a 100°C oven for 1 h, then ground and annealed in a tube furnace at 800°C for 20 h. Following the chemometric model developed by Rondinone et al. [13] the particle size was varied by adjusting the metal cation concentration in solution while keeping a 1:2 ratio between Mg and Al cations, respectively.

2.2. Characterization

X-ray diffraction patterns were collected on a Bruker D8 Advance X-ray diffractometer using Cu$K\alpha$ radiation. Particle sizes were determined from the average broadening of the five strongest diffraction peaks using the Scherrer equation. Transmission electron microscopy (TEM) experiments were performed on a JEOL 100C operating at 100 kV. Thermogravimetric analysis (TGA) and differential scanning calorimetry (DSC) were collected at a heating rate of 17°C/min to 1000°C using a Netzsch Luxx STA 409 PG. The specific surface area was measured using a Micromeritics ASAP 2000 with the BET method using nitrogen gas.

3. Results and discussion

Normal micelle microemulsion methods are able to produce $MgAl_2O_4$ nanoparticles having mean diameters from 4 to 20 nm. In order to obtain a stable microemulsion with a clear solution of the metal cations and surfactant as compared to a turbid cloudy solution, an excess of the sodium dodecyl sulfate surfactant was required. When low concentrations of the metal cations were used smaller sized $MgAl_2O_4$ nanoparticles were obtained. This is consistent with the chemometric model established by Rondinone et al. for size control of spinel ferrite nanoparticles using this normal micelle method [13]. Although the chemometric model indicated increasing the reaction temperature results in larger sized nanoparticles for the spinel ferrite systems, this was not observed in the $MgAl_2O_4$ synthesis. By testing a variety of bases such as KOH, NaOH, NH_4OH, and TPAOH, it was clear that the choice of base also did not affect the nanoparticle size. However, it is critical to maintain a pH below 11, otherwise MgO impurities are formed. This results from the formation of a soluble aluminum species, $Al(OH)_4^-$ at pH > 12, thereby creating an excess of Mg species in the precipitate.

The X-ray diffraction pattern of the dried precipitate is shown in Fig. 1a. The peaks do not match with peak positions for $MgAl_2O_4$, $Al(OH)_3$, or $Mg(OH)_2$, but agree closely with a mixed magnesium–aluminum hydroxide phase of $MgAl_2(OH)_8$ (Table 1). Surely, it is worthwhile to notice that the quality of standard X-ray diffraction pattern of $MgAl_2(OH)_8$ is not fully satisfactory. After heating the sample to just 300°C, these peaks disappear and the X-ray diffraction studies show only an amorphous phase. Bragg diffraction peaks of $MgAl_2O_4$ are observed when the samples are annealed at 800°C for 20 h (Fig. 1b). Table 2 shows clearly that the peaks match very well with the standard X-ray diffraction pattern of $MgAl_2O_4$. A typical TEM micrograph for the annealed sample shown in Fig. 2 indicates the formation of spherical particles. The size determined

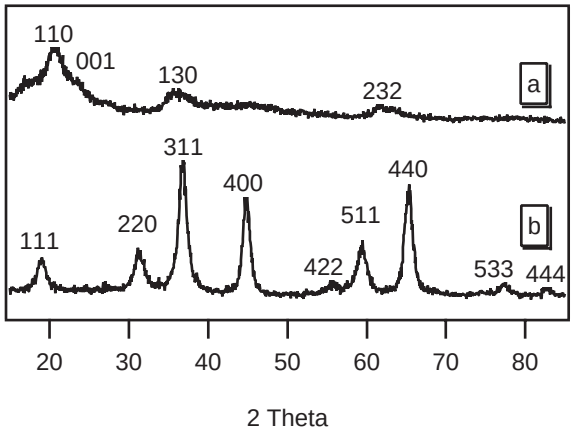

Fig. 1. X-ray diffraction patterns for (a) the initial precipitated white powder and (b) 8 nm $MgAl_2O_4$ nanoparticles formed after annealing the powder shown in panel a.

Table 1
d-spacing comparison for initial precipitate and $MgAl_2(OH)_8$

d-dried precipitate (Å)	*d*-$MgAl_2(OH)_8$ (Å)[a]	*h k l*
5.035	4.790	1 1 0
4.320	4.370	0 0 1
2.447	2.428	1 3 0
1.976	1.953	1 1 2
Not observed	1.508	−3 3 1
1.464	1.455	2 3 2

[a] Reference ICDD-PDF Card # 35-1274. Quality (i).

Table 2
d-space comparison for spinel samples

d-nanoparticle (Å)	*d*-annealed at 1100°C (Å)	*d*-$MgAl_2O_4$ (Å)[a]	*h k l*
4.673	4.684	4.660	1 1 1
2.862	2.865	2.858	2 2 0
2.439	2.441	2.437	3 1 1
Not observed	2.339	2.335	2 2 2
2.021	2.025	2.020	4 0 0
1.649	1.651	1.650	4 2 2
1.555	1.557	1.555	5 1 1
1.428	1.430	1.429	4 4 0
Not observed	1.366	1.366	5 3 1
Not observed	1.271	1.278	6 2 0
1.233	1.233	1.233	5 3 3
Not observed	1.217	1.219	6 2 2
1.166	1.168	1.167	4 4 4

[a] Reference ICDD-PDF Card #21-1152. Quality (*).

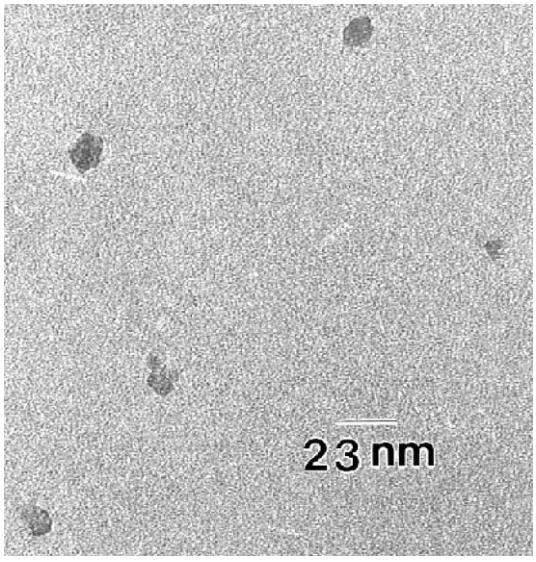

Fig. 2. TEM micrograph of 13 nm $MgAl_2O_4$ nanoparticles.

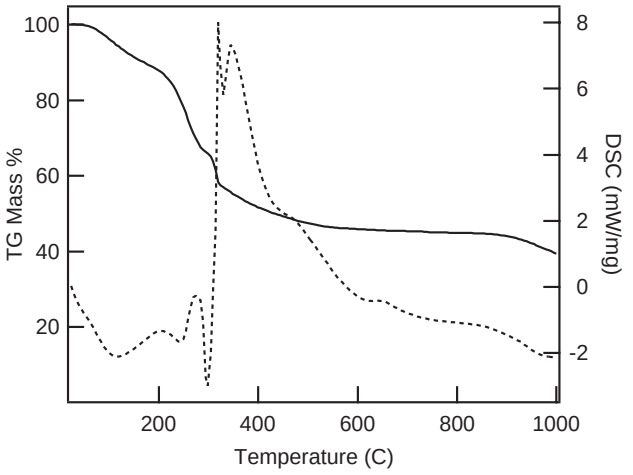

Fig. 3. TGA (solid line) and DSC (dash line) curves for precipitated products.

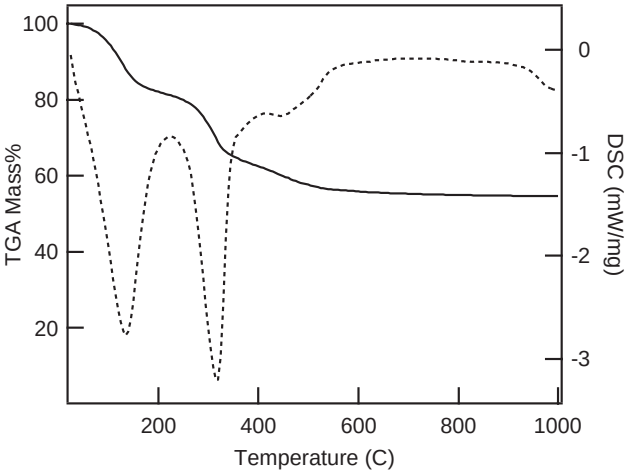

Fig. 4. TGA (solid line) and DSC (dash line) curves for $Al(OH)_3$ standard.

from the Scherrer fitting of the broadened X-ray diffraction peaks agreed well with the direct TEM observations. BET analysis of the 20 nm spinel nanoparticles yielded a surface area of 79.0 m^2/g. After the annealing temperature is raised to 1100°C, bulk phase spinel is formed (Table 2).

The TGA/DSC curves for $MgAl_2O_4$ nanoparticulate samples showed a 6% mass loss from 30°C to 150°C associated with an endothermic peak that is characteristic of the loss of adsorbed water. No other features were observed with the rising temperature, indicating once formed, this nanostructure of spinel is very stable.

The reaction pathways in the formation of $MgAl_2O_4$ nanoparticles are determined with the thermal analysis in combination with X-ray diffraction studies. The TGA/DSC curves for the initial dried precipitate are shown in Fig. 3. In the TGA curve, three clear mass losses occurred. The first was a broad 10% weight loss over the temperature range 30–200°C. The next mass loss of 25% occurred at 220–280°C and followed by a sharp 7% decrease at 310°C. At higher temperatures, the sample still slowly loses weight until ~525°C when the weight loss levels. The DSC study shows corresponding endothermic peaks over the temperature range of the first two mass losses. Around the third mass loss, a complicated overlap of endothermic and exothermic peaks was observed. A weak exotherm was also observed at ~625°C.

In order to determine what is occurring between 200°C and 450°C in the DSC curve for the initial precipitate, TGA/DSC studies were performed on $Al(OH)_3$ and $Mg(OH)_2$ samples. The results are presented in Figs. 4 and 5, respectively. Three mass loss regions are observed in the $Al(OH)_3$ sample. The first

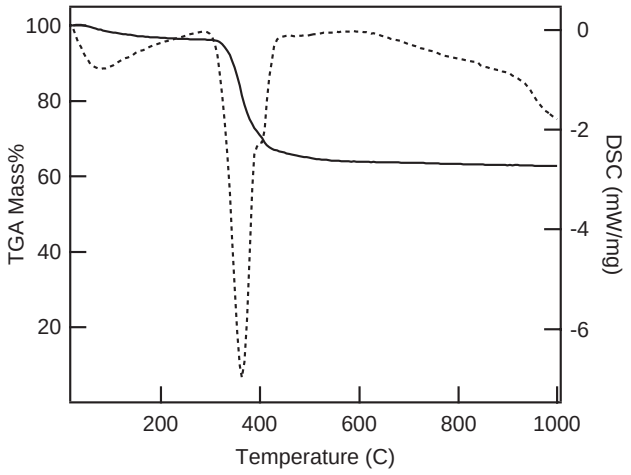

Fig. 5. TGA (solid line) and DSC (dash line) curves for $Mg(OH)_2$ standard.

two mass loss regions of 30–180°C and 220–380°C exhibit sharp endothermic peaks in the DSC curve. The third region of 380–500°C shows a weaker endotherm (Fig. 4). After the initial adsorbed water loss, the $Mg(OH)_2$ sample displayed two regions of mass loss with one in 330–370°C and a shoulder at 370–420°C with corresponding endothermic peaks in the DSC curve.

The transitions for the aluminum and magnesium hydroxide standards do not match exactly with the weight loss regions and DSC curves for the initial precipitated sample in the synthesis of $MgAl_2O_4$ nanoparticles shown in Fig. 3. However, as the X-ray diffraction studies suggest that the precipitated sample is a magnesium–aluminum mixed hydroxide, they may still provide some insights for interpreting the transitions in the precipitated products. The first region of mass loss in 30–200°C with an associated endothermic peak is likely due to the loss of adsorbed water than has been seen in all of the samples. The next two endothermic peaks with maxima at 240°C and 300°C may be associated with the loss of hydroxide from aluminum in the mixed magnesium–aluminum hydroxide sample. During the third mass loss at 310°C, a large exothermic peak begins, which is immediately followed by an endothermic transition likely resulting from the loss of hydroxide from magnesium in the mixed hydroxide. After the interruption of this transition loss, the rest of the exothermic peak continues. This large exothermic peak is likely the result of a phase transition from the $MgAl_2(OH)_8$ phase to the oxide phase. This transition is likely initiated by the loss of hydroxide associated with the endothermic peaks. Such a phase transition is consistent with the X-ray diffraction results that indicate the disappearance of hydroxide phase after annealing at 300°C. The weak exothermic peak at 650°C with no corresponding mass loss is likely the crystallization transition in which the amorphous oxide powder becomes nanocrystallites and the lattice energy is released. This is also in a very good agreement with the results from X-ray diffraction studies. At 700°C, very weak Bragg reflections are finally observed.

4. Conclusion

$MgAl_2O_4$ spinel nanoparticles with mean size of 4–20 nm can be synthesized by using normal micelle microemulsion methods. Size control is achieved simply through adjusting the metal cation concentration in the synthesis process. X-ray diffraction combined with TGA/DSC studies suggests that the initial dried white precipitate is likely a mixed magnesium–aluminum hydroxide phase which loses water to form an amorphous oxide phase at $\sim$300°C. The sample crystallizes at $\sim$650°C and form nanocrystalline $MgAl_2O_4$ spinel.

Acknowledgments

C.R.V. is partially supported by a GIT Presidential Fellowship. We thank Dr. Chris Jones and his laboratory for the access of the BET and TGA/DSC equipment. This research is supported in part by NSF (DMR-9875892), Sandia National Laboratory, and PECASE Program. TEM studies were carried out in the Electron Microscopy Center at Georgia Tech.

References

[1] H. Muraki, Y. Fujitani, Appl. Catalyst 47 (1989) 75.
[2] J. Sehested, A. Carlsson, T.V.W. Janssens, P.L. Hansen, A.K. Datye, J. Catal. 197 (2001) 200.
[3] N. Seiyama, N. Yamazoe, H. Arai, Sensor Actuator 4 (1983) 85.
[4] Y.C. Kang, J.S. Choi, S.B. Park, J. Eur. Ceram. Soc. 18 (1998) 641.
[5] O. Varnier, N. Hovnanian, A. Larbot, P. Bergez, L. Cot, J. Charpin, Mater. Res. Bull. 29 (1994) 479.
[6] V. Montouillout, D. Massiot, A. Douy, J.P. Coutres, J. Am. Ceram. Soc. 82 (1999) 3299.
[7] R.K. Pati, P. Pramanik, J. Am. Ceram. Soc. 83 (2000) 1822.
[8] M. Wang, M. Muhammed, Mater. Sci. Forum 235–238 (1997) 241.
[9] J.H. Fendler (Ed.), Nanoparticles and Nanostructured Films: Preparation, Characterization and Applications. Wiley-VCH, New York, 1998, p. 82.
[10] C. Petit, T.K. Jain, F. Billoudet, M.P. Pileni, Langmuir 10 (1994) 4446.
[11] N. Moumen, M.P. Pileni, Chem. Mater. 8 (1996) 1128.
[12] C. Liu, A.J. Rondinone, Z.J. Zhang, Pure Appl. Chem. 72 (2000) 37.
[13] A.J. Rondinone, A.C.S. Samia, Z.J. Zhang, J. Phys. Chem. B 104 (2000) 7919.